A Reverse-Selective Ion Exchange Nanocomposite Membrane: Selective Phosphate Recovery via an Outer Sphere Complexation-Diffusion Pathway

Arpita Iddya[1], Piotr Zarzycki[2], Ryan Kingsbury[3], Charmaine Khor[1], Shengcun Ma[1], Jingbo Wang[1], Ian Wheeldon[4], Zhiyong Jason Ren[5], Eric M. V. Hoek[1,6], David Jassby[1]*

[1]Department of Civil & Environmental Engineering, Institute of the Environment & Sustainability and California NanoSystems Institute, University of California, Los Angeles; Los Angeles, CA, USA

[2]Energy Geosciences Division, Lawrence Berkeley National Laboratory; Berkeley, CA, USA

[3]Department of Material Science & Engineering, University of California, Berkeley; Berkeley, CA, USA

[4]Department of Chemical and Environmental Engineering, University of California, Riverside; Riverside, CA, USA

[5]Department of Civil & Environmental Engineering and Andlinger Center for Energy & the Environment, Princeton University, NJ, USA

[6]Energy Storage and Distributed Resources Division, Lawrence Berkeley National Laboratory; Berkeley, CA, USA

*Corresponding author. Email: jassby@ucla.edu

Abstract: Polymer nanocomposite materials are used across multiple fields such as energy storage, power generation, water treatment, and resource extraction. Here, we report on a new discovery that enables phosphate-specific, reverse selectivity in cation exchange membranes. Compared to other phosphate removal/recovery methods that require chemical addition, are batch processes, and/or require multiple processing steps to recover pure phosphate, the process developed here allows for continuous recovery of phosphate with high selectivity. The specific selectivity is enabled through the in-situ growth of hydrous manganese oxide (HMO) nanoparticles (NPs) throughout a cation exchange membrane material that provide a diffusion pathway for phosphate, via specific reversible outer-sphere interaction. Upon incorporating the HMO NPs, the membrane‟s phosphate permeability increased compared to an unmodified membrane, and the membrane showed improved selectivity of 47, 100, and 20 for phosphate over other competing anions such as sulfate, nitrate, and chloride, respectively. Compared to other membrane separation processes such as an anion exchange membrane, with phosphate selectivity of 5, 1.5, and 1 for sulfate, nitrate, and chloride respectively, this modified cation exchange membrane provides improved selectivity for phosphate. By pairing the interactions of target ions with specific NPs, such nanocomposite ion exchange materials represent a new route for the synthesis of highly selective membranes capable of targeting a range of target ions for multiple applications.

Introduction

Ion selective separation membranes are used in clinical, environmental, food, and analytical applications. However, despite their extensive use, high-precision separations using membranes

remains a challenge. Fine-tuning the selectivity of membranes could increase the efficiency of existing applications and enable novel processes in new fields such as smart materials, electronics, renewable energy, and resource extraction.[1] Increasing demand for resources and the depletion of natural reserves have made it imperative to find alternate sources and technologies to meet the growing need of a modern society.[2] For instance, deposits of phosphorus and potassium, critical ingredients in fertilizers, are expected to be significantly depleted by the end of the century.[3,4] Phosphate sequestration has been achieved through precipitation (as struvite), or extraction using organic solvents. These processes require substantial infrastructure investment, high maintenance costs, and may require further separation procedures.[5] Adsorption of phosphate onto various substrates has been extensively described. Phosphate-specific sorbents include zeolities, slag (produced during steel refining), and metal (hydro)oxides.[6–8] However, the recovery of phosphate from these adsorbents requires dramatic pH swings, making the process a batch process by nature. Furthermore, the use of strong acids/bases to drive the pH swing can damage the adsorbent, reducing its lifetime and requiring frequent replenishment.[6,9] In contrast, a membrane-based phosphate separation process will enable the continuous extraction of phosphate from wastewater without the need for material regeneration or the addition of chemicals to drive a pH swing, enabling the treatment of an environmental contaminant responsible for water resource eutrophication, and the production of a valuable commodity chemical.[5,6,10,11] However, few reports on membranes that are exclusively selective towards specific anions such as phosphate exist.[3,4,12–15] In addition, while phosphate is almost always mined, the continuous extraction of phosphate ions from waste streams (such as municipal wastewater) would enable simultaneous treatment of an environmental contaminant responsible for water eutrophication and production of a valuable commodity chemical.[5,6,10,11]

Facilitated transport membranes (FTM) have been used to increase the selectivity of membranes towards specific targets by pairing the target molecule with "extractant" particles/functional groups embedded within the membrane matrix.[16–19] These extractants selectively bind with the target molecule or ion to form a complex, and transport of the target is then facilitated by either the motion of the complex (mobile carrier FTM) or hopping of the target from one carrier to another (fixed carrier/fixed-site FTM).[17] For ion separation, facilitated transport has been demonstrated using polymer inclusion or liquid membranes, but they suffer from poor stability.[20,21] To solve this stability limitation, we synthesized a novel organic/inorganic composite that enables facilitated transport of target ions through specific outer-sphere interactions between the target and an inorganic component within the membrane. Many transition metals, such as Zr, Cu, and Fe, have hard Lewis acid properties and exhibit preferential adsorptive selectivity toward phosphate.[22,23] Hydrous manganese oxide (HMO) has also been demonstrated to be an effective phosphate sorbent.[6,24–26] However, unlike other transition metals, HMO forms weaker outer-sphere complexes with phosphate, which can allow for phosphate ion hopping between adjacent manganese (di/hydro)oxide groups. [25,27] Embedding HMO NPs throughout a cation exchange membrane (CEM) (Figure 1A), which contains multiple fixed negative charges (e.g., from sulfonate groups) attached to the polymer backbone, creates a diffusion pathway for phosphate across the polymer matrix; other anions (e.g., Cl^-, NO_3^-, SO_4^{-2}) that do not form complexes with HMO are denied passage due to charge exclusion forces exerted by the CEM‟s fixed negative functional groups (Figure 1B).

Here we report on the synthesis, testing, and characterization of a facilitated transport mixed matrix membrane capable of selectively extracting phosphate from a mixed anion solution. The membrane is fabricated via *in situ* oxidation of manganese in a CEM to form HMO NPs

embedded throughout the CEM (HMO-CEM). Through a combination of experimental and theoretical analysis, we characterize the transport properties of the hybrid material towards phosphate, explain the mechanisms responsible for phosphate transport, and determine that the rate-limiting step for phosphate transport is the complexation reaction between the HMO NPs and phosphate ions. This study explores the fundamental principles behind the selective transport of ions, and paves the way towards a new class of selective membrane materials.

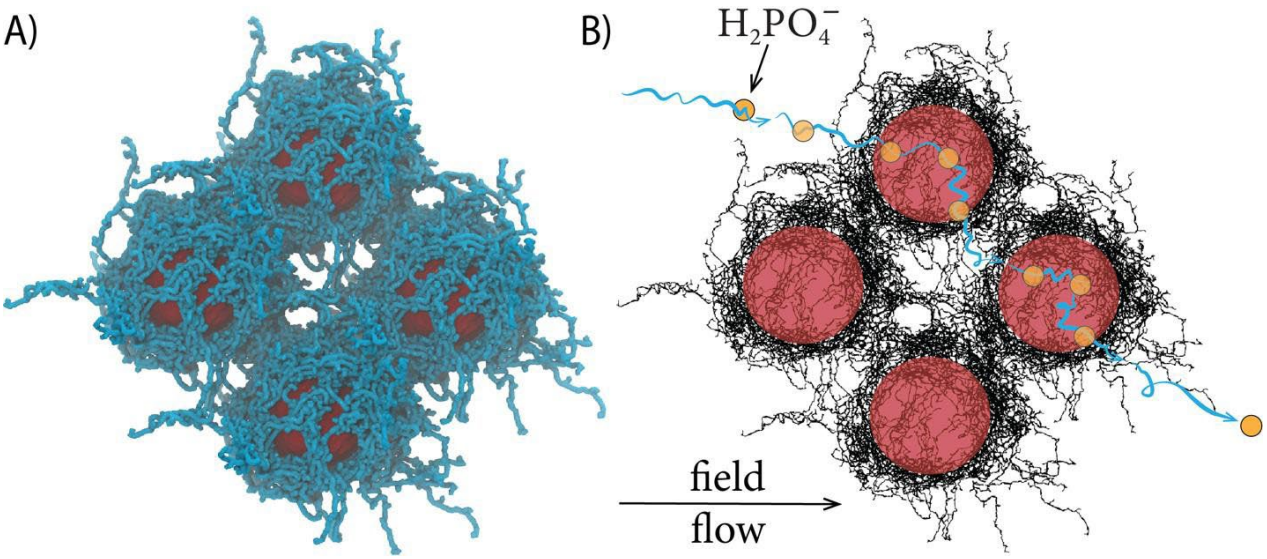

Figure 1: Molecular representation of the HMO-CEM membrane (A) and proposed mechanism of selective phosphate transport. The weak outer-sphere complexes $H_2PO_4^-$/HMO are formed within the Stern part of the EDL, which are relatively mobile and can migrate around HMO particle if subjected to external driving force like flow or weak electric field. The $H_2PO_4^-$ ions jump from one HMO particle to another through the intergel solution phase, that is, through the fluid-saturated micro and mesopore spaces. The phosphate ions adsorbed to HMO diffuse within the particle EDL in the direction of the flow or applied electric field.

Results & Discussion

HMO loading for the two membranes, high loading HMO-CEM and low loading HMO-CEM, was determined to be 117 mg MnO_2/g of membrane and 69 mg MnO_2/g of membrane, respectively. The effect of increasing the HMO loading on the membrane properties such as ion exchange capacity, water uptake, and volume fraction have been described in the SI (Table S1).

Visual investigation of the membranes demonstrates the successful modification of the CEM with HMO; while the pristine CEM is a white, slightly transparent material, the HMO-CEM is transformed into a solid black material (Figure 2A, B). The structure and uniformity of the HMO immobilized within the membrane was investigated using transmission electron microscopy (TEM), and X-ray photoelectron spectroscopy (XPS), and X-ray diffraction (XRD). Cross-sectional TEM micrographs of the HMO-CEM clearly show the presence of HMO NPs distributed uniformly throughout the membrane, with an average size of approximately 79.4 ±23.1 nm, while TEM micrographs of the unmodified CEM show no distinguishing features (Figures 2C, D). XRD analysis of the particles and HMO-CEM membrane showed no distinguishing peaks associated with the HMO particles, suggesting that the particle had an

amorphous structure (Figure S1). The XPS spectrum of the modified HMO-CEM shows a distinct Mn peak at ~ 642.8 eV, demonstrating the successful incorporation of Mn, at least at the surface of the material (Figure 2E).[28,29] Fourier transform infrared spectroscopy (FTIR) peaks (Figure 2F) of the HMO-CEM show a weak broad band with a peak centered around 3400 cm^{-1} resulting from the stretching vibrations of –OH following HMO loading, a broadening of a peak at 600 cm^{-1}, and two additional peaks at 712 cm^{-1} and 681 cm^{-1}, corresponding to the MnO_x stretching, bending, and wagging vibrations, respectively.[30,31]

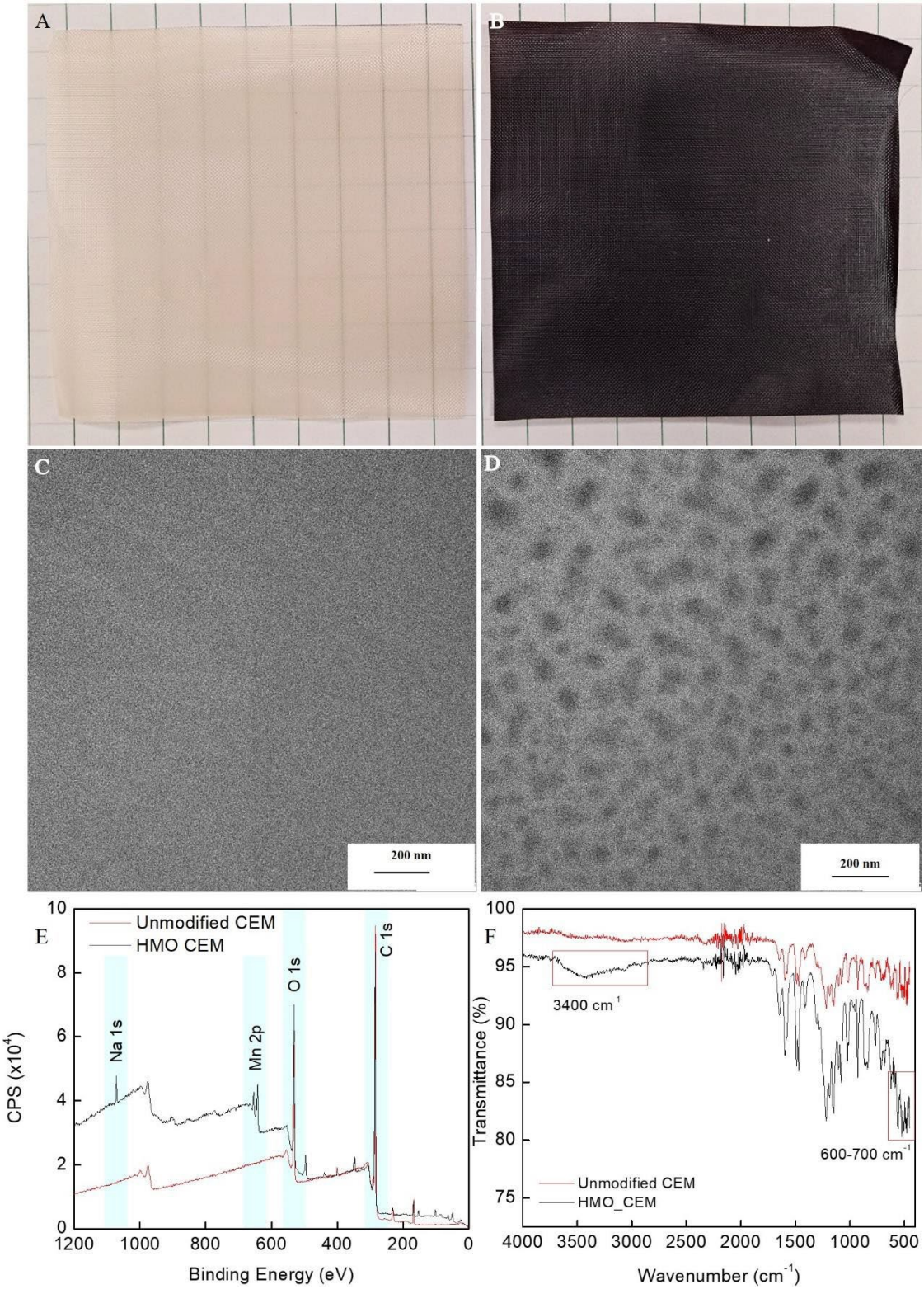

Figure 2: Photographs of the A) unmodified CEM and B) HMO-CEM. Cross-sectional TEM micrographs for C) unmodified CEM and D) HMO-CEM show Mn nanoparticles embedded uniformly within the HMO-CEM matrix with an average particle size of ~79.4 ±23.1 nm. XPS spectra (E) shows the Mn peak of the HMO-CEM at ~642.8 eV, demonstrating successful

incorporation of Mn into the CEM; and FTIR spectra (F) shows a weak band at 3400 cm^{-1} resulting from stretching of –OH, and peak broadening at 600-700 cm^{-1} corresponding to MnO_x stretching and bending vibrations.

Transport and Selectivity of Phosphate using HMO-CEM

Phosphate transport across an unmodified CEM and HMO-CEM with two different HMO loadings shows that the transport rate is highly dependent on HMO loading. The setup for these experiments is described in supplementary materials (section 1) and follows the schematic in Figure S2. As seen in Figure 3A, the unmodified CEM showed extremely low transport rates ($0.8x10^{-8}$ $mol \cdot m^{-2} \cdot s^{-1}$, Figure 3A). This result is not surprising considering the high concentration of fixed, negatively charged sulfonate groups within the polymer matrix, which prevent the uptake and passage of phosphate anions. Phosphate transport across the HMO-CEM (with no applied potential, i.e., Donnan dialysis, and with an applied potential, i.e., electro-dialysis) is shown in Figure 3A and S. For both HMO-CEM loadings, the phosphate concentration in the receiving compartment increased over time. For the high HMO loading case, under the effect of the combined driving forces (concentration gradient + electric field; black triangles, Figure 3A), phosphate concentration in the receiving (anolyte) compartment increased for the first three hours, with a flux of $21.7x10^{-8}$ $mol \cdot m^{-2} \cdot s^{-1}$ (while this flux is low compared to anion fluxes through anion exchange membranes, the flux can be increased by increasing the driving force and, in addition, the membrane exhibits dramatically enhanced selectivity towards phosphate – more on this below). However, after three hours the flux declined to $5.4x10^{-8}$ $mol \cdot m^{-2} \cdot s^{-1}$. We speculate that this flux decline is a result of pH-induced changes in phosphate speciation. As the experiment progressed, the pH of the anolyte rapidly declined from 5.5 at t=0 h to 2.9 at t=3 h as a result of water electrolysis (Figure 3A). Under the applied electric field, protons generated at the anode migrate towards the cathode, penetrating the HMO-CEM as they migrate between the two chambers, and reducing the inter-membrane pH. Since the pKa_1 of phosphate is 2.1, as the pH approaches this level, fewer phosphate molecules complexed with the HMO NPs are ionized ($H_2PO_4^-$ vs. H_3PO_4), making them less susceptible to the electrophoretic driving force and slowing their transport across the membrane. Under Donnan dialysis conditions, the pH decline was not as significant (possibly as a result of accumulation of phosphate ions) compared to the pH under electro-dialysis conditions (pH declined to 4.7 from 5.7 after 7 hours). Because the pH never dropped to extreme levels under these conditions, phosphate flux was constant throughout the experiment ($5.1x10^{-8}$ $mol \cdot m^{-2} \cdot s^{-1}$). This is further evidenced by the lower phosphate flux and pH drop under an applied potential when using an HMO-CEM with low HMO loading ($2.6x10^{-8}$ $mol \cdot m^{-2} \cdot s^{-1}$) (Figure 3A, section 2.5 of supplementary materials). The pH in the anolyte, for the low HMO loading experiments, declined to 3.3 over the duration of the experiment, and the flux remained fairly constant as compared to that using a high-loading HMO-CEM. The lower flux for the low-loading HMO-CEM highlights the importance of the embedded HMO NPs in enabling phosphate transport across the CEM.

Membrane selectivity towards phosphate

Membrane selectivity experiments revealed superior selectivity of the HMO-CEM in transporting phosphate over other competing anions (Figure 3B). The experiments were conducted under electrodialysis conditions with a mixture of electrolytes, all at an initial concentration of 1 mM, in the catholyte and DI water as the anolyte. For the unmodified CEM, extremely low transport of all anions was observed with a slight preference for Cl^- transport over other species. (Figure 3C). This result is attributed to the large concentration of negatively

charged sites on the CEM. We also tested the selectivity of an anion exchange membrane (AEM). The AEM showed high transport rate for all anions, with little selectivity of phosphate over other anions (Figure S3A). The separation factor of phosphate over other anions was determined to be 1 (for chloride), 5 (for sulfate), 1.5 (for nitrate) (Figure S3B). In contrast to both, the HMO-CEM enabled phosphate to pass through the membrane (with a flux of 11.9E-8 $mol/m^2/s$), while still rejecting all other anion species (Figure 3D). While the unmodified CEM shows a gradual increase in Cl^- concentration over time, the HMO-CEM shows an increase in Cl^- concentration only in the first hour followed by a much lower Cl transport rate. This initial increase in Cl^- concentration for HMO-CEM is attributed to the chloride ions added into the matrix as a result of using NaOCl during membrane preparation. Moreover, the drop in Cl^- transport rate across the HMO-CEM as compared to the unmodified CEM could be due to the decrease in the intergel (the region of the CEM that allows co-ion transport) volume upon introduction of HMO NPs.[32,33] Based on the fluxes of the different anions measured in these experiments, the separation factor of phosphate over chloride, nitrate, and sulfate was determined to be 20, 100 and 47, respectively. The large standard deviation in separation factors for the competing anions are due to the low concentrations of these ions (near the detection limit of the IC), resulting in large variability in concentration measurement, as shown in Figure S4.

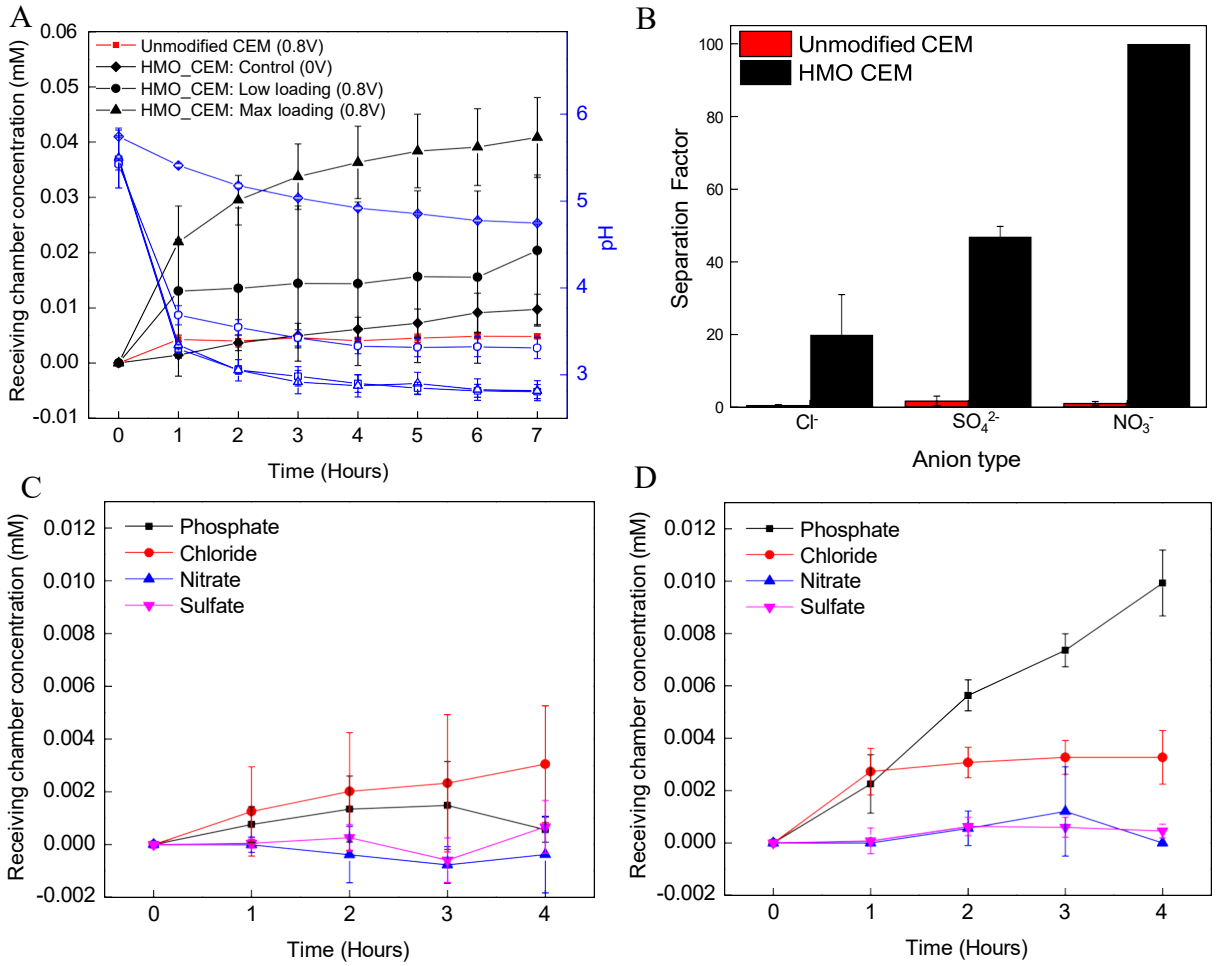

Figure 3: A) Phosphate concentration and pH in the receiving chamber for an unmodified CEM, high-loading HMO-CEM, and low-loading HMO-CEM in the presence and absence of an applied potential. The feed solution was composed of 0.1 M NaH_2PO_4, while 0.05M Na_2SO_4 was used as the receiving solution. A potential of 0.8 V *vs*. Ag/AgCl (2V cell potential) was applied across two Pt wires used as electrodes in the feed (cathode) and permeate (anode) chambers. (B) Phosphate selectivity over competing anions (Cl^-, SO_4^{2-}, and NO_3^-) for an unmodified and HMO-CEM. Phosphate concentration in the receiving chamber for the (C) unmodified CEM, and (D) HMO-CEM for an equimolar solution (1mM) of NaCl, Na_2SO_4, $NaNO_3$, and NaH_2PO_4 as the feed solution, and 18MΩ de-ionized water as the permeate; a potential of 0.8V Vs Ag/AgCl (2V cell potential) was applied across two Pt wires used as electrodes in the feed (cathode) and permeate (anode) chambers. Error bars represent standard deviations.

Molecular Dynamics Simulation

To understand the interactions and transport of the ions through the HMO-CEM membrane on the molecular level, we carried out molecular dynamics simulations of $H_2PO_4^-$ and Na^+ ions in configurations that resemble the gel and intergel phases of the HMO-CEM (section 2.2 in supplementary text). The all-atoms simulation protocol imposes a severe restriction on the size of the simulation cell. Consequently, the size of the embedded HMO particle and pore are scaled

down compared to the experimental conditions. Specifically, the diameter of the simulated HMO particle is 10 nm, and the ions can explore the micro- and mesopore spaces of the HMO-CEM composite membrane. In our model, we constrained the size of the HMO particle to 10 nm to minimize the computational load. However, we do not anticipate that the nature of the phosphate-HMO interaction is impacted by the particle size, although we have not verified this. The impact of nanoparticle size is beyond the scope of this paper and is a topic for future studies. The system size is still sufficient to reveal the modes of interactions/complexation by polymer and particle and the molecular mechanism of phosphate transport through the HMO-CEM membrane. In Figure 4A-B, we show molecular snapshots of the HMO-CEM system and the molecular model of the model ion exchange polymer molecule.

The values of the diffusion coefficients of the $H_2PO_4^-$ and Na^+ ions obtained from the molecular dynamics trajectories are listed in Table S3 (averages over 10 independent simulation runs), where each simulation started from a slightly different initial configuration. The diffusion coefficients for the ions in the aqueous solution are representative of the intergel solution phase, whereas those along the HMO-CEM are representative of the gel phase. As can be seen, the calculated ion diffusivities in the gel phase are approximately three ($H_2PO_4^-$) and two (Na^+) times lower than their diffusivities inside the intergel solution phase. The presence of the HMO particle increases the mobility of phosphate by about 20%, but has a negligible effect on the mobility of sodium, whose mobility drops by 8% (Table S3). The electric field accelerates the ionic mobility within the gel phase of HMO-CEM by 21% and 27% for phosphate and sodium ions, respectively.

The ions have the lowest mobility in the system composed of electrolyte solution in contact with the HMO particle (Table S3). Both sodium and phosphate adsorb at the HMO particle surface, forming outer-sphere complexes (Figure 4D). The presence of the negatively charged polymeric matrix accelerates ion transport due to disruption of the weak electrical double layer formed around the HMO particle. Because the negatively charged polymeric matrix attracts Na^+ and repels $H_2PO_4^-$ ions, the Na^+ ions are pulled away from the HMO vicinity, and $H_2PO_4^-$ ions are pushed away from the polymer. Critically, $H_2PO_4^-$ ion interaction with the particle weakens due to the depletion of Na^+ ions around the HMO particle, and electrostatic attraction between $H_2PO_4^-$ and Na^+ ions accumulated near negatively charged groups in the ion exchange polymer. As a result, the mobility of $H_2PO_4^-$ increases nonlinearly in the gel phase of HMO-CEM compared to the cases of CEM or HMO-only systems (Table S3). This nonlinearity is due to the complexity of the ion pathways across the HMO-CEM matrix. First, ion fluxes through the micro and mesopores differ due to the variation in the solvent properties, different proximity of the polymer chains and particle surfaces, and pore-size-dependent permeability. Second, an ion‟s ability to diffuse against the field or in the direction perpendicular to the field decreases with increasing voltage. As the strength of the field increases, the thermal motion of ions diminishes, and the translation along the field lines dominates their dynamics. If the ion reaches the HMO surface, it can diffuse around it as an outer-sphere complex. However, if the ion becomes trapped in the dense polymer pocket with no exit channel, it will not escape by diffusing against the electric field lines. The voltage-dependent diffusivities (Figure 4C) capture this phenomenon, showing subtle deviation from the expected exponential dependence. While the diffusivities of the individual phosphate ions vary in any given simulation, the simulation shows that the slowest ions are moving through the polymeric channels while the fastest move through the intergel

solution phase or near the HMO particles. The molecular dynamics simulations provide a molecular-level understanding of phosphate transport through the HMO-CEM membrane. Simulations confirm experimental observations (section 2.2 in supplementary text) that $H_2PO_4^-$ ions are forming only outer-sphere complexes with HMO, enabling their uptake onto the HMO-CEM material, and facilitating their diffusion across the membrane. This transport is driven by an electric field or concentration gradient across the membrane. The simulations also confirm that phosphate mobility is much higher in the HMO-CEM compared to the pure CEM.

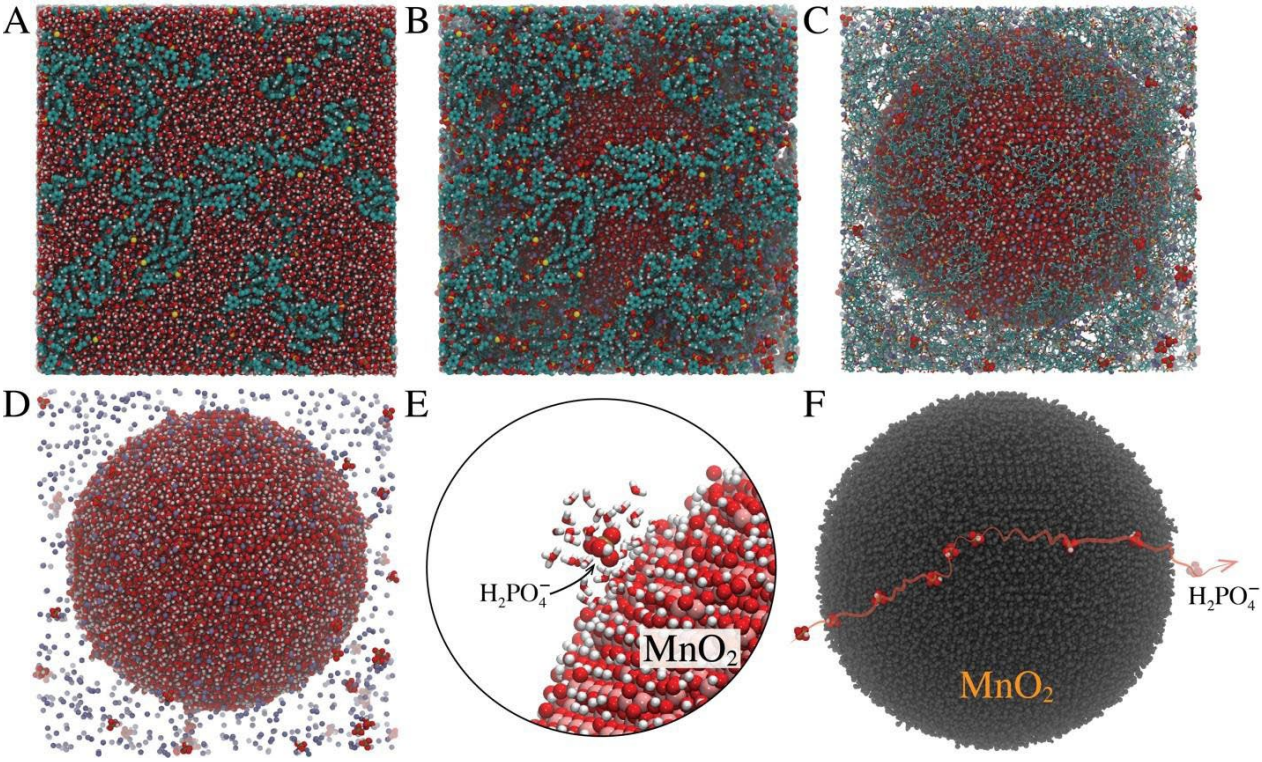

Figure 4: Example of the simulation cell used in the molecular dynamics simulations: A) all atoms shown as vdw-spheres, B) water molecules are hiden, C) water moelcules hidden and polymer represented by the ball-and-stick model, D) only HMO particlesa and ions are shown, E) example of the H2PO4- ion with its hydration water in the outer-sphere complex geometry, F) illustration of the diffusion pathway of adsorbed $H_2PO_4^-$.

Phosphate transport model

Using our experimental observations, a model describing ion transport across the HMO-CEM was developed based on the microheterogeneous model for ion exchange membranes (section 2.1 in supplementary text).[34,35] The model was used to predict the flux and transport number for phosphate, and was then used to estimate the HMO loading needed to increase phosphate transport across the membrane. Phosphate flux and transport number were calculated using equations S9- S25, with the concentration profile for the ions throughout the membrane given by equation eq. S26. The parameter, n, in equation S26, and the structural parameter, α, in equations S11 & S22, were treated as adjustable parameters and fit to the model. The value of n (Eq. S26) defines the concentration profile across the membrane thickness; an $n = 1$ value corresponds to a linear concentration profile, with increasing n values corresponding to a more rapid, exponential decline (Figure S5).[36] The value of α can vary from –1 to 1, and represents the connectivity of the gel and intergel phases of the microhetergoneous model, with $\alpha = -1$ referring to the phases

connected in a series, while an $\alpha = 1$ refers to a parallel connection.[34] We obtained the lowest root mean square error values for the transport number and flux of the unmodified and low-loading HMO-CEM with $n = 10$ and $\alpha = 0.3$, compared to our experimentally-determined values (Table S3); the predicted vs. observed phosphate flux values can be seen in Figure 5A. Although the flux predictions for the unmodified and low-loading HMO-CEM are within 30% of the experimental results, the predicted flux for the high-loading HMO-CEM, using the same n and α values, is almost 2 times lower than the experimental flux (data not shown). However, since hydration of a polymeric membrane leads to the formation of micro and meso-pores, which swell strongly as water intercalates between the polymeric chains within the membrane,[37] it is possible that the modification of the membrane by the *in situ* growth of HMO NPs affects the internal membrane structure and changes the α parameter, and by extension, the concentration profile of co-ions within the membrane (the *n*-parameter). By adjusting the parameters n and α to 5 and 0.7, respectively, the predicted flux had an error of about 7% (Figure 5A). Physically, $n = 5$ implies that the concentration decline of the phosphate anion across the high-loading HMO-CEM is more gradual compared to that of an unmodified membrane, where an $n = 10$ value yielded the best fit (Figure 5A). This implies that the high concentration of ion-exchange groups in an unmodified membrane limit the presence of co-ions within the membrane, which are thus present primarily near the feed/membrane interface leading to an exponential decline across the membrane thickness (i.e., higher *n* values). In contrast, in the HMO-CEM, due to phosphate‟s ability to form outer-sphere complexes with HMO NPs (section 2.6 in SI), phosphate concentrations throughout the material are higher resulting in a linear decline in concentration as one moves away from the membrane/feed interface. Similarly, introduction of a large quantity of HMO NPs alters the internal structure of the membrane; an increased value of α ($\alpha = 0.7$) represents a more parallel orientation of the gel and intergel phases in relation to the transport axis (perpendicular to the membrane surface) as compared to that of an unmodified membrane.

The ion transport numbers predicted by the model were compared to those obtained from the experiments in Figure 5B. Transport numbers describe the fraction of current carried by a particular ion species relative to the overall current passing through the system (eq. S23). For the case of phosphate transport across unmodified and modified CEMs, the model predicts that the addition of HMO to the CEM matric increases the fraction of current carried by phosphate. Moreover, it also accurately calculates transport numbers for the unmodified and low loading HMO-CEM. Thus, for these membranes, our simplifying assumption that accounts for sodium and proton transport during the experiments (see eq. S23 and S24) is valid. However, the model under-predicts the transport number for the high loading HMO-CEM by ~30%, thus indicating that at higher HMO loadings the simplifying assumption fails to appropriately account of fraction of phosphate transport and thus its transport number.

The model predicts a higher gel-phase diffusion coefficient for anions over cations, by nearly two orders of magnitude (Table 1). This could be attributed to the electrostatic attraction between cations and the polymeric fixed charges, which the anions/co-ions do not experience.[38] While this may seem counter-intuitive (since the flux of cations is much higher than that of anions), the higher flux can be explained by Donnan exclusion, which causes counter ions to partition into the membrane at a higher rate than co-ions, resulting in higher counter ion concentrations within the membrane. Thus, cations are transported across by interaction with the fixed charges in the gel phase of the membrane, while the anions are transported through the electroneutral solution

present in the intergel phase and the cation and anion transport are correlated (coupled) to maintain charge-neutrality of the fluid phase. In the HMO phase, the diffusion coefficient of phosphate is higher than that of cations. Importantly, the specific interactions of phosphate ions with the HMO particles enables their partitioning into and diffusion across the HMO-CEM, resulting in a higher diffusion coefficient for the phosphate anions. As a result, phosphate is transported across the membrane through the intergel phase by „hopping" along the HMO NPs.

Finally, the model was used to estimate the HMO loading that would yield a phosphate flux comparable to phosphate flux through an anion exchange membrane. Increasing the HMO loading of a CEM affects its properties including water uptake, ion exchange capacity, the diffusion coefficient of salt through the membrane, and the volume fraction occupied by the NPs within the membrane. However, since most of these values were obtained from experiments and used as inputs into the model, extrapolating the model to accurately predict phosphate flux at higher HMO loading is riven with uncertainty. During the formation of HMO NPs within the CEM (according to the reactions listed in 1.2), Na^+ displaces the Mn on the charged fixed sites, forming the eventual HMO particles in the vicinity of the gel phase, which could possibly explain the decrease in ion exchange capacity with increase in the HMO loading (Table S1). Assuming that the ion exchange capacity decreases and f_{int} (volume fraction of intergel phase in the membrane) increases linearly with f_p (volume fraction of particles within the membrane), we can estimate that for f_p = 0.07, the flux of phosphate would increase to 1.04×10^{-5} $mol \cdot m^{-2} \cdot s^{-1}$, comparable to the cation flux through CEM and anion flux through an anion exchange membrane.[39–41] It is also possible that NP size could affect the performance of HMO-CEM. We speculate that a decrease in NP size would lead to decrease in the ion exchange capacity since the smaller sized NPs would block the fixed charges and decrease their charge exclusion effect on the co-ion. However, our model does not account for NP size and the experimental work is beyond the scope of this study.

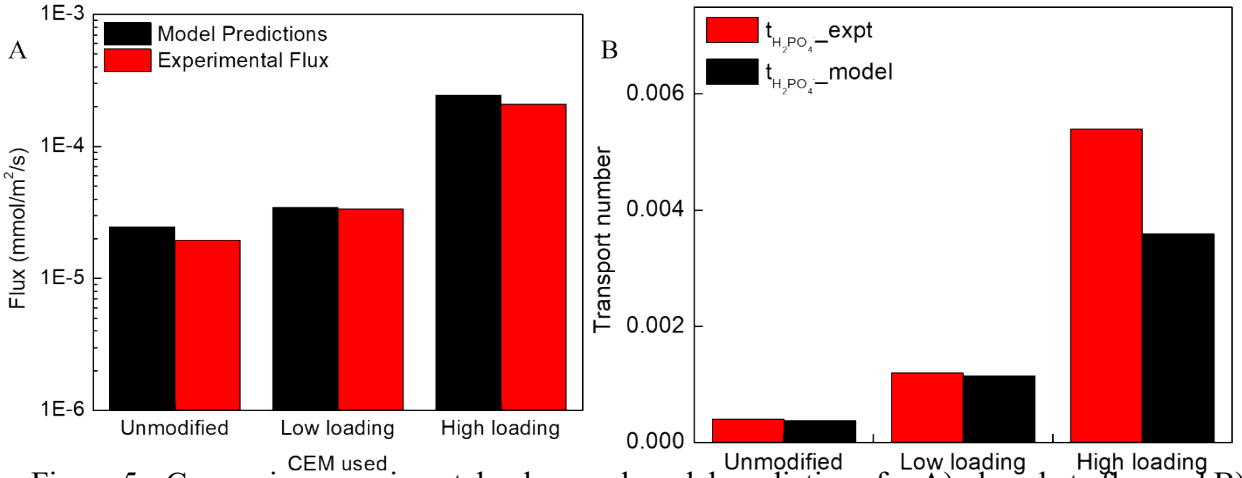

Figure 5: Comparing experimental values and model predictions for A) phosphate flux and B) phosphate transport number.

Table 1: Results from the microheterogenous model

			[m²/s]	[m²/s]
	[mM]	[M]		

Unmodified	0.24	4.49	3.00×10^{-9}	2.65×10^{-11}	0.0004
Low-loading	0.35	3.07	3.01×10^{-9}	3.87×10^{-11}	0.0011
High-loading	0.62	2.91	3.03×10^{-9}	4.06×10^{-11}	0.0036

In this study, we successfully synthesized, characterized, and tested a new class of membranes that allow for selective transport of phosphate across a cation exchange membrane. Selective separation is achieved by exploiting the outer-sphere complexation reaction between phosphate and the embedded HMO NPs within the membrane. This technique paves the way towards a novel approach to specific ion recovery, which utilizes similar complexation interactions between the target ions and the embedded extractant groups in ion exchange membranes, while the fixed charges prevent passage of competing co-ions. Other ionic species such as lithium, uranium, gold, and metals that exist as oxy-anions (including arsenic, vanadium, and hexavalent chromium) could possibly be extracted by employing appropriate NPs that complex with the target ion. Thus, these membranes demonstrate an innovative technology desirable from the perspective of both water quality (due to toxicity) and resource recovery.

Methods

Materials. A commercial CEM (Fumasep FKS-PET-130, FuelCellStore, College Station, TX) and AEM (Fumasep FAS-PET-130, FuelCellStore, College Station, TX) were used for this study and were either used without further modifications or modified as described below. Manganese chloride tetrahydrate ($MnCl_2.2H_2O$, Reagent grade, Sigma Aldrich), manganese (II) sulfate monohydrate ($MnSO_4.H_2O$, 99%, extra pure, ACROS Organics), sodium hydroxide (NaOH, pellets, certified ACS, Fisher), Sodium hypochlorite (NaOCl, 7.1% available chlorine, Clorox), sodium phosphate monobasic monohydrate ($NaH_2PO_4.H_2O$, 98%, ACS reagent, Sigma Aldrich), sodium sulfate (Na_2SO_4, Certified ACS, Fisher), sodium nitrate ($NaNO_3$, Certified ACS, Fisher), and sodium chloride (NaCl, ACS grade, Fisher) were used as received.

1.2 Preparation of HMO-CEM. HMO was loaded into the CEM, to form the Mixed Matrix Membrane (MMM) HMO-CEM, by using a three step process, modified from Qing and Pan.[42,43] First, the CEM in its dry form was immersed in a solution containing 2.5 M $MnCl_2 \cdot 4H_2O$ and 3 M $MnSO_4 \cdot H_2O$ (5.5 M total Mn^{2+} concentration) for either 1 hour or 24 hours (to form a low-loading and high-loading (fully loaded) HMO-CEM, respectively). As a result, Mn^{2+} in solution exchange with H^+ in the membrane:[42]

( )

Next, an oxidizing solution was prepared by dissolving NaOH into a sodium hypochlorite solution to prepare a 1M NaOH solution with 7% NaOCl (w/w). The Mn-exchanged membrane was then immersed into the oxidizing solution for either 1 hour or 24 hours, for the low- and high-loading HMO-CEM, respectively, and the Mn^{2+} counter-ions were oxidized to produce HMO (unbalanced):

( ) ( )

Finally, The HMO-CEM was then washed with copious amounts of deionized (DI) water and vacuum dried at 50 ºC for at least 12 hours. The prepared HMO-CEM was immersed in a 0.5 M $NaH_2PO_4.H_2O$ solution prior to experiments.

1.3 Membrane Characterization. The surface morphology and cross-sectional structure of the unmodified CEM and HMO-CEM were studied using scanning electron microscopy (SEM) equipped with energy dispersive X-ray spectroscopy (EDX) (ZEISS Supra 40VP SEM), and transmission electron microscopy (TEM; TF20 High Resolution EM, FEI). X-ray photoelectron spectroscopy (XPS; Kratos Axis Ultra DLD spectrometer equipped with a monochromatic Al Kα X-ray source) was used to characterize the elemental composition of the membrane surface and the oxidation state of manganese; all binding energies were referenced to the C 1s peak at 284.8 eV. Chemical bonds in the membranes were evaluated using Fourier transform infrared spectroscopy (FTIR) operated in transmission mode (Thermo Scientific FTIR iS10 Smart iTR Basic), with a Ge prism as an internal reflection element. FTIR was also used to evaluate possible Mn-P interactions in the phosphate loaded HMO-CEM; for this, the sample was prepared by soaking the membrane in 0.5M $NaH_2PO_4 \cdot H_2O$ solution for 24 hours, rinsed with DI water, and dried at 50 ºC for 12 hours. To measure the total amount of HMO NPs incorporated, the HMO loaded membranes were weighed before and after placing them in a high temperature furnace. The weight of the ash is subtracted to achieve the weight of HMO nanoparticles. The HMO quantity is normalized to the membrane surface area to calculate HMO loading.

References

1. Jackson, D. T. & Nelson, P. N. Preparation and properties of some ion selective membranes: A review. *J. Mol. Struct.* **1182**, 241–259 (2019).
2. Uliana, A. A. *et al.* Ion-capture electrodialysis using multifunctional adsorptive membranes. *Science (80-.).* **372**, 296–299 (2021).
3. Paltrinieri, L. *et al.* Hybrid polyelectrolyte-anion exchange membrane and its interaction with phosphate. *React. Funct. Polym.* **133**, 126–135 (2018).
4. Zhou, Y., Hu, C., Liu, H. & Qu, J. Potassium-Ion Recovery with a Polypyrrole Membrane Electrode in Novel Redox Transistor Electrodialysis. *Environ. Sci. Technol.* **54**, 4592–4600 (2020).
5. Harris, S. M. *et al.* Gadolinium Complex for the Catch and Release of Phosphate from Water. *Environ. Sci. Technol.* **51**, 4549–4558 (2017).
6. Pan, B. *et al.* New strategy to enhance phosphate removal from water by hydrous manganese oxide. *Environ. Sci. Technol.* **48**, 5101–5107 (2014).
7. Blaney, L. M., Cinar, S. & SenGupta, A. K. Hybrid anion exchanger for trace phosphate removal from water and wastewater. *Water Res.* **41**, 1603–1613 (2007).
8. Bowden, L. I., Jarvis, A. P., Younger, P. L. & Johnson, K. L. Phosphorus removal from waste waters using basic oxygen steel slag. *Environ. Sci. Technol.* **43**, 2476–2481 (2009).
9. Pitakteeratham, N., Hafuka, A., Satoh, H. & Watanabe, Y. High efficiency removal of phosphate from water by zirconium sulfate-surfactant micelle mesostructure immobilized on polymer matrix. *Water Res.* **47**, 3583–3590 (2013).
10. Liu, R. *et al.* Effective and selective adsorption of phosphate from aqueous solution via trivalent-metals-based amino-MIL-101 MOFs. *Chem. Eng. J.* **357**, 159–168 (2019).
11. Pan, B. *et al.* Development of polymer-based nanosized hydrated ferric oxides (HFOs) for enhanced phosphate removal from waste effluents. *Water Res.* **43**, 4421–4429 (2009).
12. Tor, A. Removal of fluoride from water using anion-exchange membrane under Donnan dialysis condition. *J. Hazard. Mater.* **141**, 814–818 (2007).
13. Khor, C. M. *et al.* Electrically Mediated Membrane Pore Gating via Grafted Polymer

Brushes. *ACS Mater. Lett.* **1**, 647–654 (2019).
14. Elimelech, M. & Phillip, W. A. The future of seawater desalination: Energy, technology, and the environment. *Science* **333**, 712–717 (2011).
15. Paltrinieri, L. *et al.* Functionalized Anion-Exchange Membranes Facilitate Electrodialysis of Citrate and Phosphate from Model Dairy Wastewater. *Environ. Sci. Technol.* **53**, 2396–2404 (2019).
16. Noble, R. D. & Koval, C. A. Review of Facilitated Transport Membranes. *Mater. Sci. Membr. Gas Vap. Sep.* 411–435 (2006). doi:10.1002/047002903X.ch17
17. Li, Y. *et al.* Facilitated transport of small molecules and ions for energy-efficient membranes. *Chem. Soc. Rev.* **44**, 103–118 (2015).
18. Tang, C. & Bruening, M. L. Ion separations with membranes. *J. Polym. Sci.* **58**, 2831–2856 (2020).
19. Ounissi, T., Dammak, L., Larchet, C., Fauvarque, J. F. & Selmane Bel Hadj Hmida, E. Novel lithium selective composite membranes: synthesis, characterization and validation tests in dialysis. *J. Mater. Sci.* **55**, 16111–16128 (2020).
20. Almeida, M. I. G. S., Cattrall, R. W. & Kolev, S. D. Recent trends in extraction and transport of metal ions using polymer inclusion membranes (PIMs). *J. Memb. Sci.* **415–416**, 9–23 (2012).
21. Scindia, Y. M., Pandey, A. K. & Reddy, A. V. R. Coupled-diffusion transport of Cr(VI) across anion-exchange membranes prepared by physical and chemical immobilization methods. *J. Memb. Sci.* **249**, 143–152 (2005).
22. Ramakrishnam Raju, M. V., Harris, S. M. & Pierre, V. C. Design and applications of metal-based molecular receptors and probes for inorganic phosphate. *Chem. Soc. Rev.* **49**, 1090–1108 (2020).
23. Acelas, N. Y., Martin, B. D., López, D. & Jefferson, B. Selective removal of phosphate from wastewater using hydrated metal oxides dispersed within anionic exchange media. *Chemosphere* **119**, 1353–1360 (2015).
24. Fransiscus, Y., Widi, R. K., Aprilasti, G. O. & Yuharma, M. D. Adsorption of phosphate in aqueous solutions using manganese dioxide. *Int. J. Adv. Sci. Eng. Inf. Technol.* **8**, 818–824 (2018).
25. Yao, W. & Millero, F. J. Adsorption of phosphate on manganese dioxide in seawater. *Environ. Sci. Technol.* **30**, 536–541 (1996).
26. Kawashima, M., Tainaka, Y., Hori, T., Koyama, M. & Takamatsu, T. Phosphate adsorption onto hydrous manganese(IV) oxide in the presence of divalent cations. *Water Res.* **20**, 471–475 (1986).
27. Mustafa, S., Zaman, M. I. & Khan, S. Temperature effect on the mechanism of phosphate anions sorption by β-MnO2. *Chem. Eng. J.* **141**, 51–57 (2008).
28. Nesbitt, H. W. & Banerjee, D. Interpretation of XPS Mn(2p) spectra of Mn oxyhydroxides and constraints on the mechanism of MnO2 precipitation. *Am. Mineral.* **83**, 305–315 (1998).
29. Yang, Z. *et al.* Vertically-aligned Mn(OH)2 nanosheet films for flexible all-solid-state electrochemical supercapacitors. *J. Mater. Sci. Mater. Electron.* **28**, 17533–17540 (2017).
30. Parikh, S. J. & Chorover, J. FTIR spectroscopic study of biogenic Mn-oxide formation by Pseudomonas putida GB-1. *Geomicrobiol. J.* **22**, 207–218 (2005).
31. Wang, X. & Andrews, L. Infrared spectra of M(OH) (M = Mn, Fe, Co, Ni) molecules in solid argon and the character of first row transition metal hydroxide bonding. *J. Phys.*

Chem. A **110**, 10035–10045 (2006).
32. Stenina, I., Golubenko, D., Nikonenko, V. & Yaroslavtsev, A. Selectivity of transport processes in ion-exchange membranes: Relationship with the structure and methods for its improvement. *Int. J. Mol. Sci.* **21**, 1–33 (2020).
33. Jashni, E., Hosseini, S. M., Shen, J. N. & Van der Bruggen, B. Electrochemical characterization of mixed matrix electrodialysis cation exchange membrane incorporated with carbon nanofibers for desalination. *Ionics (Kiel).* **25**, 5595–5610 (2019).
34. Porozhnyy, M., Huguet, P., Cretin, M., Safronova, E. & Nikonenko, V. Mathematical modeling of transport properties of proton-exchange membranes containing immobilized nanoparticles. *Int. J. Hydrogen Energy* **41**, 15605–15614 (2016).
35. Zhang, B., Gao, H., Xiao, C., Tong, X. & Chen, Y. The trade-off between membrane permselectivity and conductivity: A percolation simulation of mass transport. *J. Memb. Sci.* **597**, 117751 (2020).
36. Kingsbury, R. S. & Coronell, O. Modeling and validation of concentration dependence of ion exchange membrane permselectivity: Significance of convection and Manning‟s counter-ion condensation theory. *J. Memb. Sci.* **620**, 118411 (2020).
37. Kononenko, N. *et al.* Porous structure of ion exchange membranes investigated by various techniques. *Adv. Colloid Interface Sci.* **246**, 196–216 (2017).
38. Lopez, M., Kipling, B. & Yeager, H. L. Ionic Diffusion and Selectivity of a Cation Exchange Membrane in Nonaqueous Solvents. *Anal. Chem.* **49**, 629–632 (1977).
39. Rottiers, T., De la Marche, G., Van der Bruggen, B. & Pinoy, L. Co-ion fluxes of simple inorganic ions in electrodialysis metathesis and conventional electrodialysis. *J. Memb. Sci.* **492**, 263–270 (2015).
40. White, N., Misovich, M., Yaroshchuk, A. & Bruening, M. L. Coating of Nafion membranes with polyelectrolyte multilayers to achieve high monovalent/divalent cation electrodialysis selectivities. *ACS Appl. Mater. Interfaces* **7**, 6620–6628 (2015).
41. Hosseini, S. M., Jeddi, F., Nemati, M., Madaeni, S. S. & Moghadassi, A. R. Electrodialysis heterogeneous anion exchange membrane modified by PANI/MWCNT composite nanoparticles: Preparation, characterization and ionic transport property in desalination. *Desalination* **341**, 107–114 (2014).
42. Su, Q. *et al.* Fabrication of polymer-supported nanosized hydrous manganese dioxide (HMO) for enhanced lead removal from waters. *Sci. Total Environ.* **407**, 5471–5477 (2009).
43. Pan, B. C. *et al.* Highly effective removal of heavy metals by polymer-based zirconium phosphate: A case study of lead ion. *J. Colloid Interface Sci.* **310**, 99–105 (2007).